Journal of Hydrology (2008) 353, 189–200

available at www.sciencedirect.com

ScienceDirect

journal homepage: www.elsevier.com/locate/jhydrol

A joint model for rainfall–runoff: The case of Rio Grande Basin

Romy R. Ravines [a], Alexandra M. Schmidt [a,*], Helio S. Migon [a], Camilo D. Rennó [b]

[a] *Departamento de Métodos Estatísticos, Instituto de Matemática, Universidade Federal do Rio de Janeiro, Caixa Postal 68530, Rio de Janeiro, RJ, CEP 21945-970, Brazil*
[b] *Coordenação Geral de Observação da Terra, Divisão de Processamento de Imagens, Instituto Nacional de Pesquisas Espaciais, São José dos Campos, SP 12227-010, Brazil*

Received 10 July 2007; received in revised form 4 February 2008; accepted 12 February 2008

KEYWORDS
Bayesian paradigm;
Dynamic models;
Transfer functions;
Spatio-temporal;
Spatial change of support

Summary We present an analysis of runoff and rainfall data from Rio Grande, a basin located in the northeast of Brazil. The main challenges we face here are: (i) to model runoff and rainfall jointly, taking into account their different spatial units, (ii) to use stochastic models where all the parameters have physical interpretations, and (iii) to model these processes in their original scale, without assuming any transformation to attain normality of these variables.

The intrinsically uncertain nature of these hydrological processes makes Bayesian analysis natural in this field. Our approach is based on dynamic models. The effect of rainfall on runoff is modeled through a transfer function, whereas the amount of rainfall is obtained after fitting a spatio-temporal model and dealing with the change of support problem. Besides the computational effort to implement the proposed models, some methodological novelties are also implemented.

The data consist of monthly series from January 1984 to September 2004, at a runoff station and nine rainfall stations irregularly located in a drainage area of 37522.48 km^2. Model assessment, spatial interpolation and temporal predictions were part of our analysis. The results show that our approach is a promising tool for rainfall–runoff analysis.

Introduction

One of the challenges that hydrologists and operators of water resource systems face is to predict the runoff given the rainfall. The intrinsically uncertain nature of these

* Corresponding author. Tel.: +55 21 2562 7505x204; fax: +55 21 2562 7374.
E-mail addresses: romy@dme.ufrj.br (R.R. Ravines), alex@im.ufrj.br (A.M. Schmidt), migon@im.ufrj.br (H.S. Migon), camilo@dpi.inpe.br (C.D. Rennó).
URL: http://www.dme.ufrj.br/~alex (A.M. Schmidt).

0022-1694/$ - see front matter © 2008 Elsevier B.V. All rights reserved.
doi:10.1016/j.jhydrol.2008.02.008

hydrological processes makes Bayesian analysis natural in this field, whenever statistical problems are considered (Rios-Insua et al., 2002).

In this paper we present an alternative strategy for dealing with the spatial and temporal features of two of the most important hydrological variables: runoff and rainfall. Our goals are: (i) to model both variables jointly, taking into account their different spatial units, (ii) to use stochastic models where all the parameters have physical interpretations, and (iii) to model these processes in their original scale, without assuming any transformation to attain normality of these variables.

Several types of stochastic models have been proposed for the rainfall–runoff relationship, based on deterministic models or on classical time series analysis. Two important classes of stochastic models applied to river flow analysis are: transfer function and regime switching. Transfer function modeling is flexible and has been mainly used in the form of ARMAX models (see, for example, Sales (1989) and Capkun et al. (2001)). Markov Switching time series models, as in Lu and Berliner (1999) have been recently introduced. These approaches are not ideal, because data transformation is needed and the parameters do not have interpretation in physical terms. Also, in all the previous proposed models, the measurement errors and uncertainty associated with rainfall are not explicitly accounted for. This is because models must describe the rainfall–runoff process on a drainage catchment area basis. However, in practice, precipitation is measured at more than one monitoring station within a basin, thus some procedure is needed in order to approximate the precipitation for the whole basin. There are some widely used methods that make use of polygons to determine the influence area of each station. The total basin's precipitation is computed as a weighted mean of the precipitation measured at each station. The problem with this kind of procedure is that the uncertainty of this estimation is not taken into account when modeling runoff as a function of rainfall.

Here we propose a joint model for both variables: rainfall and runoff. For rainfall, we use spatio-temporal models, like in Sansó and Guenni (2000). For runoff, we use non-normal and non-linear Bayesian dynamic models. In particular, we extend the models presented by Migon and Monteiro (1997). Additionally, to approximate the basin's rainfall, we solve the implicit change of support problem (see Cressie (1993) and Gelfand et al. (2001) for further details). The models presented here allow us to represent parsimoniously a complex system of physical processes, which fit and forecast rather well, without losing the physical interpretation of their parameters.

Inference procedure is performed under the Bayesian paradigm. Markov Chain Monte Carlo (MCMC) methods are used to assess posterior distributions of the unknown quantities. Since the proposed models can be computationally intensive when fitted with MCMC techniques, we sought to use algorithms that perform thousands of iterations in a few minutes. In particular we focused in the runoff model, for which we used a sampling scheme recently proposed by Ravines et al. (2007). It combines the conjugate updating of West et al. (1985) for dynamic models in the exponential family, with the backward sampling of Frühwirth-Schnater (1994).

This paper is organized as follows. In Section ''Rio Grande Basin, Brazil: Runoff–Rainfall Data'' we briefly describe the Brazilian data we used to illustrate our methodology. Section ''Individual models for rainfall and runoff'' is devoted to a general discussion of some particular individual models for runoff and rainfall previously proposed. In Section ''A simultaneous model for rainfall–runoff'' the joint model proposed here is described and the main aspects of the inference procedure are discussed. In Section ''Modeling in practice: Inference procedure'' we present the results of the analysis of the Rio Grande basin data, and in Section ''Concluding remarks'' we offer some concluding remarks.

Rio Grande Basin, Brazil: Runoff–Rainfall Data

The Rio Grande basin is located in the northeast of Brazil, in Bahia State, a dry sub-humid area with tropical weather. The region under study is between the 11° and 13° South parallels and 43° 30′ and 46° 30′ West meridians. This basin has a drainage area of 37522.48 km^2. The available dataset consists of monthly recorded series from August 1984 to September 2004 (242 months), at one runoff station (Taguá), and nine rainfall stations irregularly located in the drainage area. Fig. 1a shows the location of each station and Fig. 1b shows the data for the four monitoring stations marked in 1a.

From Fig. 1b we observe that there are distinct wet and dry periods annually: the rainy season begins in November and lasts through March, with the average accumulated monthly rainfall over 275 mm; while the dry season is from late April until October, when the average monthly rainfall rarely exceeds 10 mm. Most of the basin is sparsely vegetated and relatively flat, meaning that altitude has no influence in the hydrological regime. Thus, it is not taken into account in our models.

Individual models for rainfall and runoff

Two of the main features of the rainfall–runoff relationship are: it is basically non-linear and the current runoff depends on previous runoff plus current and past precipitation. It can be assumed that there is no feedback between runoff and rainfall, so a transfer function model seems to be a natural option for fitting and forecasting this phenomenon. Besides, runoff is a non-negative variable and its time series can be non-stationary. Thus, we propose the use of non-linear and non-normal dynamic models to handle this kind of data.

Let Y_t be the runoff and X_t be the precipitation at time t. The rainfall–runoff relationship can be represented by

$$Y_t \sim p(Y_t|\mu_t, \phi_t), \quad t = 1, 2, \ldots \tag{1a}$$

$$g(\mu_t) = f_1(\alpha_t, E_t) \tag{1b}$$

$$E_t = f_2(E_{t-1}, \ldots, E_0, X_t), \tag{1c}$$

where $p(Y_t|\mu_t, \phi_t)$ is a density function for a non-negative random variable; μ_t is the expected value of Y_t; ϕ_t represents other parameters of $p(Y_t|\mu_t, \phi_t)$; α_t is a basic level and E_t is the total effect of rainfall at time t; and $g(\cdot)$, $f_1(\cdot)$ and $f_2(\cdot)$ are known functions describing the dynamics of the hydrological process. Time varying parameters and stochastic variations affecting E_t are particular cases of (1).

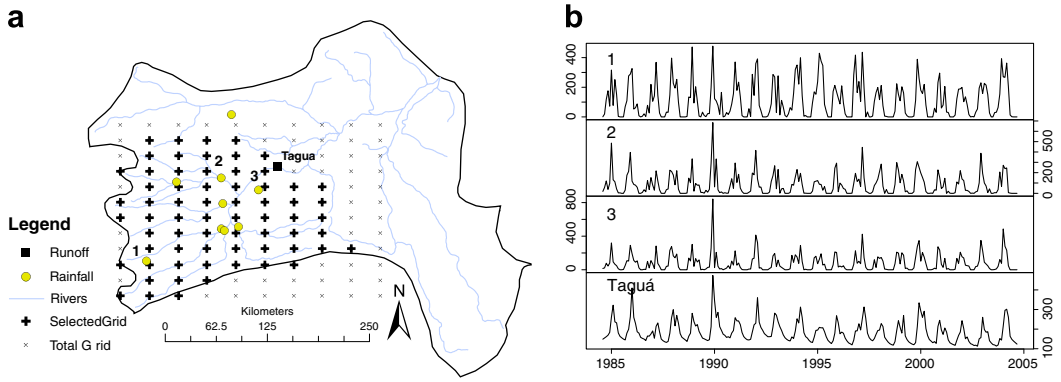

Figure 1 Rio Grande Basin: (a) Locations of the monitoring stations; (b) Time series of monthly runoff at Taguá, and rainfall at sites 1, 2, and 3 (marked in (a)).

A dynamic transfer function model

Following the assumptions made in Migon and Monteiro (1997), the relationship between runoff and rainfall can be expressed as a transfer function model. The model in (1) assumes that the expected value of the total runoff generated (streamflow), μ_t, or a function of it, say $g(\mu_t)$, can be written as a baseflow α_t, which depends on the water table level, plus an effect of current and past precipitation E_t, which is $\mu_t = \alpha_t + E_t$. The effect of precipitation is expected to decay between time $t-1$ and t by a rate $\rho_t \in (0,1)$. This parameter plays the role of a recharge or rainfall effect memory rate and depends on the geomorphology and land-use/land-cover of the basin. Therefore, it should be (almost) constant over time. Temporal changes in this parameter can be explained by drastic changes in, e.g., soil and/or vegetation characteristics. Since E_{t-1} represents the effect of precipitation before time t, a fraction of current rainfall, say $\gamma_t X_t$, can be added to compute the rainfall effect at time t. The parameter γ_t measures the instantaneous effect of rainfall and is mainly associated with overland flow speed. This parameter has a particular temporal dynamic: it is strongly related to the soil infiltration capacity and the rainfall interception by the vegetation. After a rainy period, the soil is saturated and the overland flow will be high. However, after a dry period, the soil absorbs a great part of water and the overland flow will decrease. Also, when vegetation grows, the leaf density becomes high, increasing the rainfall interception and consequently decreasing its instantaneous effect on the discharge. Alternatively, if ϑ_t is the maximum expected precipitation effect, then $\vartheta_t > \mu_t$ and the remaining possible runoff is $\vartheta_t - (\alpha_t + \rho E_{t-1})$. Therefore E_t, in (1c), can be expressed as one of the following expressions:

$$E_t = \rho_t E_{t-1} + \gamma_t X_t \tag{2a}$$

$$E_t = \rho_t E_{t-1} + [1 - \exp(-\kappa_t X_t)][\vartheta_t - (\alpha_t + \rho_t E_{t-1})]. \tag{2b}$$

Eqs. (2a) and (2b) support the hypothesis that the precipitation effect decays exponentially with time. See Panel (a) of Fig. 2, where for illustrative purposes, we assume $X_t = 0$ for all t, except at $t = 5$, when $X_t = 1$. We notice that the effect of X_t on E_t dies off after $t = 10$. In Eq. (2a), the greater the amount of rainfall, the greater is its returns to runoff. Panel (b) of Fig. 2 gives an example of such situation when $\rho = 0.70$ and $\gamma = 0.30$. This hypothesis is known as proportional returns. On the other hand, in Eq. (2b), the greater the amount of rainfall, the smaller is its effect and, moreover, this effect has an upper limit. This function is pictured in Panel (c) of Fig. 2), where we assumed $\rho = 0.70, \gamma = 0.30, \kappa = 0.10, \vartheta = 10.00$ and $\alpha = 5.00$. The latter is known as the diminishing returns hypothesis (Migon and Harrison, 1985).

Modeling rainfall

Note that the input X_t in model (1) corresponds to the precipitation of a whole basin, that is, a unique measure of rainfall is needed at each time t. However, in many situations, precipitation is observed in more than one station

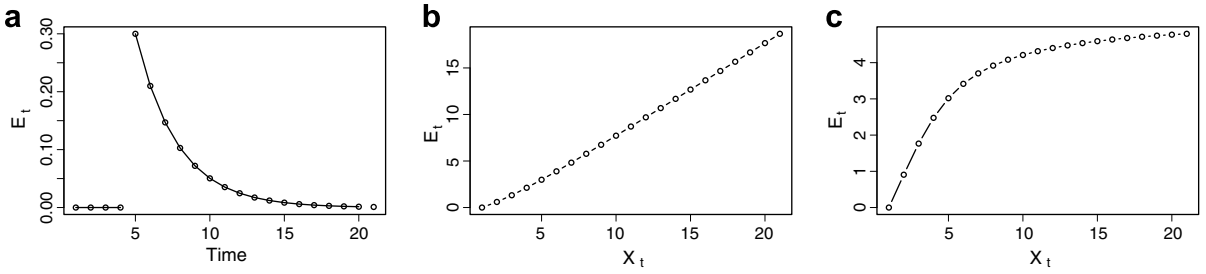

Figure 2 Examples of the shapes of the transfer functions in (2a) and (2b). In all cases, it was assumed $\rho = 0.70$ and $\gamma = 0.30$. In panel (a) $X_t = 1$ if $t = 5$ and $X_t = 0$ otherwise. In Panel (c) it was further assumed: $\kappa = 0.10, \vartheta = 10.00$ and $\alpha = 5.00$.

within a basin. So, the total rainfall for time t, X_t, should be obtained from the solution of the spatial change of support problem. The change of support problem is concerned with inference about the values of the variable over areal units (block data) different from those at which it has been observed (Gelfand et al., 2001). Areal rainfall can be viewed as a sum over point rainfall data, because it is a continuous univariate spatial process.

Let $\{X_t(s), s \in B \subset \mathbb{R}^2, t = 1, 2, \ldots\}$ be a spatial random field at discrete time t. Here, $X_t(s) \geqslant 0$ is a random variable that represents the amount of rainfall at time t and location s. So, the rainfall for a given basin or region B, X_t, is given by

$$X_t = \int_B X_t(s)\mathrm{d}s, \tag{3}$$

where B is the basin's domain. In particular, we assume $X_t(s)$ follows a truncated normal distribution and, as suggested by Sansó and Guenni (2000), is represented by the following spatio-temporal model:

$$X_t(s) = \begin{cases} w_t(s)^{\beta} & \text{if } w_t(s) > 0, \\ 0 & \text{if } w_t(s) \leqslant 0 \end{cases} \quad s \in B, \tag{4a}$$

$$\boldsymbol{w}_t = \boldsymbol{Z}_t + \boldsymbol{v}_t \quad \boldsymbol{v}_t \sim GP(\boldsymbol{0}, \tau^2 \boldsymbol{I}), \tag{4b}$$

$$\boldsymbol{Z}_t = \boldsymbol{F}'\theta_t + \epsilon_t \quad \epsilon_t \sim GP(\boldsymbol{0}, \sigma^2 \boldsymbol{V}), \tag{4c}$$

$$\theta_t = \boldsymbol{G}\theta_{t-1} + \omega_t \quad \omega_t \sim GP(\boldsymbol{0}, \boldsymbol{W}_t), \tag{4d}$$

where GP denotes a Gaussian process and $\tau^2\boldsymbol{I}$ and $\sigma^2\boldsymbol{V}$ are the covariance matrices of $\boldsymbol{w}_t$ and $\boldsymbol{Z}_t$, respectively. Here $\boldsymbol{I}$ denotes the identity matrix. The term $\boldsymbol{v}_t$ is a random error whose variance, τ^2, is known as the nugget effect (Cressie, 1993). The variance of each $Z_t(.)$ is denoted by σ^2, and its correlation function is represented by $\varrho(\|s_i - s_j\|, \lambda) = V_{ij}$, which depends on λ, and on the Euclidean distance, $\|s_i - s_j\|$, between the locations s_i and s_j. In this case, $\boldsymbol{F}'\theta_t$ represents a polynomial trend and $\boldsymbol{G}$ is the evolution matrix of the parameters θ_t. An alternative way of modeling rainfall is to use a model derived from a mixture taking into account the excess of zeros (dry season), as in Velarde et al. (2004) and Fernandes et al. (in press).

Fitting Equations (1) and (3) jointly is our proposed approach. Our formulation covers a wide class of relationships. It is very flexible and all of its parameters have a clear interpretation. Moreover, all the uncertainty involved in the physical process is clearly taken into account, as rainfall is not considered as a known quantity.

A simultaneous model for rainfall–runoff

Assume that we have runoff data from T time periods and rainfall data from S locations over a basin B, observed during the same time period. Let Y_t and X_t be the basin's runoff and rainfall at time t, respectively. Then, $\boldsymbol{Y}$ denotes the basin's runoff time series, that is, $\boldsymbol{Y} = (Y_1, \ldots, Y_T)\prime$, and $\boldsymbol{X}$ denotes the basin's rainfall time series, that is, $\boldsymbol{X} = (X_1, \ldots, X_T)'$. Let $X_t(s_i)$ denotes rainfall at time t and gauged location s_i. Then, $\boldsymbol{X}_t(\boldsymbol{s}) = (X_t(s_1), \ldots, X_t(s_S))\prime$ is the rainfall observed at time t over the S gauged locations (for each time t), and $\boldsymbol{X}(s_i) = (X_1(s_i), \ldots, X_T(s_i))\prime$ is the rainfall time series observed at gauged site s_i (for each location). And, $\boldsymbol{X}(\boldsymbol{s}) = (\boldsymbol{X}(s_1), \ldots, \boldsymbol{X}(s_S))\prime$, with $\boldsymbol{s}$ denoting the vector of gauged locations $(s_1, \ldots, s_S)$, is the matrix of rainfall observed at the S locations over T time periods. The joint distribution (see Appendix A for details) of $\boldsymbol{Y}$, $\boldsymbol{X}$ and $\boldsymbol{X}(s)$ is given by

$$p(\boldsymbol{Y}, \boldsymbol{X}, \boldsymbol{X}(\boldsymbol{s})|\boldsymbol{\Theta}) = p(\boldsymbol{Y}|\boldsymbol{X}, \boldsymbol{X}(\boldsymbol{s}), \boldsymbol{\Theta}_Y)p(\boldsymbol{X}, \boldsymbol{X}(\boldsymbol{s})|\boldsymbol{\Theta}_X), \tag{5}$$

where $\boldsymbol{\Theta} = (\boldsymbol{\Theta}_Y, \boldsymbol{\Theta}_X)$, $\boldsymbol{\Theta}_Y$ denotes the parameters in (1) and $\boldsymbol{\Theta}_X$ denotes the parameters in (4). Note that in (5) the joint distribution of runoff and rainfall is modeled through the conditional distribution of runoff given rainfall, times the marginal distribution of rainfall (Schmidt and Gelfand, 2003). Also,

$$\begin{aligned} p(\boldsymbol{Y}, \boldsymbol{X}, \boldsymbol{X}(\boldsymbol{s})|\boldsymbol{\Theta}) &= \prod_{t=1}^{T} p(Y_t|X_t, \boldsymbol{X}_t(\boldsymbol{s}), \boldsymbol{\Theta}_Y)p(X_t, \boldsymbol{X}_t(\boldsymbol{s})|\boldsymbol{\Theta}_X) \\ &= \prod_{t=1}^{T} p(Y_t|X_t, \boldsymbol{X}_t(\boldsymbol{s}), \boldsymbol{\Theta}_Y)p(X_t|\boldsymbol{X}_t(\boldsymbol{s}), \boldsymbol{\Theta}_X) \\ &\quad \times \prod_{i=1}^{S} p(X_t(s_i)|\boldsymbol{\Theta}_X). \end{aligned} \tag{6}$$

Gelfand et al. (2001) proposed to approximate $p(X_t, \boldsymbol{X}_t(\boldsymbol{s})|\boldsymbol{\Theta}_X)$ by using Monte Carlo integration. They proposed to sample a set of observations in S_B locations, independent and uniformly distributed over B, and compute

$$\widehat{X}_t = \sum_{i=1}^{S_B} \widehat{X}_t(s_i) \quad i = 1, \ldots, S_B, \tag{7}$$

where $\widehat{X}_t(s_i)$ is the predicted value for rainfall at the ith location from a regular interpolation grid (with locations $s_1^*, s_2^*, \cdots, s_{S_B}^*$) of S_B points constructed inside the bounds of B. Consequently, (7) is a Monte Carlo approximation of (3).

The predictive distribution needed for the spatial interpolation of $X_t(s_i)$, at a new set of locations, for instance, $(X_t(s_1^*), \ldots, X_t(s_{S_B}^*))'$, is given by

$$p(\boldsymbol{X}(s')|\boldsymbol{X}(s)) = \int p(\boldsymbol{X}(s')|\boldsymbol{X}(s), \boldsymbol{\Theta}_X)p(\boldsymbol{\Theta}_X|\boldsymbol{X}(s))p(\boldsymbol{\Theta}_X)d\boldsymbol{\Theta}_X, \tag{8}$$

where $\boldsymbol{\Theta}_X$ denotes all the parameters in (4).

Following the Bayesian paradigm, model specification is complete after assigning the prior distribution of all the unknowns. From Bayes' theorem we obtain the kernel of the posterior distribution, which does not have an analytical closed form. Samples from the posterior distribution can be obtained via Markov chain Monte Carlo (MCMC) methods (Gamerman and Lopes, 2006). Based on the expressions above, the inference procedure via MCMC can be done in the following steps:

(1) Fit a spatio-temporal model for rainfall, $\boldsymbol{X}(\boldsymbol{s})$, observed at S gauged locations over B;
(2) Build a regular grid over the domain and obtain a sample of the rainfall over the basin, $\mathbf{X}$, following Eqs. (7) and (8). That is, first obtain a sample from the predictive distribution of $\boldsymbol{X}(\boldsymbol{s})$ (for each point of the interpolation grid), then use these values to approximate the rainfall over the basin using Eq. (7);
(3) For each sampled value of rainfall over the basin, X_t, obtained in the previous step, fit the runoff model as in Eq. (1).

In particular, we assume that runoff follows either a log-normal or a gamma distribution. In the case of the log-normal distribution, we applied a log transformation and the algorithm forward filtering backward sampling (FFBS) of Frühwirth-Schnater (1994) was used to obtain samples of the posterior distribution of interest. In the case of the gamma distribution, we propose the use of a sampling scheme which combines the conjugate updating of West et al. (1985) for dynamic models in the exponential family, with the backward sampling of Frühwirth-Schnater (1994). This algorithm is called conjugate updating backward sampling (CUBS); details are found in Ravines et al. (2007). We note that in non-normal transfer function models CUBS significantly reduces the computing time needed to attain convergence of the chains, and is also very simple to implement.

Modeling in practice: inference procedure

We applied the approach described in Section ''Individual models for rainfall and runoff'' to the rainfall data from the nine stations and the runoff series observed at Taguá station in the Rio Grande basin. Specifically, we used the function in (2a) for E_t in (1c) and a multivariate dynamic linear model (see West and Harrison, 1997, Chapter 16) for the temporal evolution of the parameters in (4). For a better explanation, we reproduce our whole, general, model in (9)

$$Y_t|X_t \sim p(\mu_t,\phi) \quad t=1,\ldots,T \tag{9a}$$
$$\log(\mu_t) = \alpha_t + E_t \tag{9b}$$
$$E_t = \rho E_{t-1} + \gamma_t X_t + w_t \quad w_t \sim N(0,\sigma_E^2) \tag{9c}$$
$$\alpha_t = G_\alpha \alpha_{t-1} + w_{\alpha,t} \quad w_{\alpha,t} \sim N(0,\sigma_\alpha^2) \tag{9d}$$
$$\gamma_t = G_\gamma \gamma_{t-1} + w_{\gamma,t} \quad w_{\gamma,t} \sim N(0,\sigma_\gamma^2) \tag{9e}$$
$$X_t = \sum_{j=1}^{S_B} \widehat{X}_t(s_j) \quad j=1,\ldots,S_B \tag{9f}$$
$$X_t(s_i) = \begin{cases} w_t(s_i)^\beta & \text{se } w_t(s_i) > 0 \\ 0 & \text{se } w_t(s_i) \leqslant 0 \end{cases} \quad i=1,\ldots,S \tag{9g}$$
$$\boldsymbol{w}_t = \boldsymbol{z}_t + \boldsymbol{v}_t \quad \boldsymbol{v}_t \sim GP(\boldsymbol{0},\tau^2\boldsymbol{I}) \tag{9h}$$
$$\boldsymbol{z}_t = \boldsymbol{F}'\boldsymbol{\theta}_t + \boldsymbol{\epsilon}_t \quad \boldsymbol{\epsilon}_t \sim GP(\boldsymbol{0},\sigma^2\boldsymbol{V}_t) \tag{9i}$$
$$\boldsymbol{\theta}_t = \boldsymbol{G}\boldsymbol{\theta}_{t-1} + \boldsymbol{\varepsilon}_t \quad \boldsymbol{\varepsilon}_t \sim GP(\boldsymbol{0},\boldsymbol{W}_t) \tag{9j}$$
$$\boldsymbol{\theta}_0 \sim N(\boldsymbol{0},\boldsymbol{100I}), \tag{9k}$$

where $p(\mu_t,\phi)$ is the log-normal or gamma distribution and ϕ corresponds to the precision parameter of the former and the shape parameter of the latter. In (9g)–(9k), S is the number of monitoring sites and S_B is the number of points in the interpolation grid. $X_t(s_i)$ denotes the rainfall at time $t=1,\ldots,T$ and site $s_i=s_1,\ldots,s_S$, $w_t(s_i)$ is a latent Gaussian variable, β is an unknown power, $\boldsymbol{w}_t$ is a vector of dimension S that stacks the S observations made at time t, τ^2 is a nugget effect, $\sigma^2>0$ and $\boldsymbol{V}_t$ is a spatial correlation matrix of dimension S. Here we assume that $V_{s_i,s_{i'}} = \exp(-\lambda d_{s_i,s_{i'}})$, that is, an exponential decay correlation where λ controls the decay rate, $\lambda>0$ and $d_{s_i,s_{i'}}$ is the Euclidean distance between sites s_i and $s_{i'}$, $i,i'=1,\ldots,S$. In (9i)–(9k), $\boldsymbol{F}'$ is an $S\times k$ matrix, $\boldsymbol{G}$ is a $k\times k$ matrix and $\boldsymbol{\theta}$ is a vector of dimension k. The elements of $\boldsymbol{\theta}$ are such that $\boldsymbol{\theta}_t=(\boldsymbol{\theta}_{t1},\boldsymbol{\theta}_{t2})\prime$, where $\boldsymbol{\theta}_{t1}$ is a sub-vector that describes the spatial trend and $\boldsymbol{\theta}_{t2}$ describes the seasonal effects. Eqs. (9d) and (9e) represent possible time evolutions of α and γ, respectively. In practice, just one of these equations is considered and depends on the features of the basin under study.

Prior distributions and full conditional distributions

In general, we used fairly vague prior distributions. However, since all the involved parameters have physical interpretations, an elicitation procedure could be done. For the parameters of the spatio-temporal model in (9g)–(9k), we set $p(\boldsymbol{\theta}_0,\sigma^2,\varsigma^2,\lambda,\beta) = p(\boldsymbol{\theta}_0)p(\sigma^2)p(\varsigma^2)p(\lambda)p(\beta)$, where $\varsigma^2=\tau^2/\sigma^2$, $p(\boldsymbol{\theta}_0)$ is an $S-$ variate normal distribution with mean $\boldsymbol{0}$ and an identity covariance matrix, $N_S(\boldsymbol{0},\boldsymbol{I})$ and $p(\sigma^2)$ is an improper distribution, $1/\sigma^2$. On the other hand, $p(\varsigma^2),p(\lambda)$ and $p(\beta)$ are gamma densities with parameters $(0.001,0.001)$, $(2.00,6/1.86)$ and $(12,4)$, respectively. The hyper-parameters for λ were selected according to the premise that at half of the maximum distance between the observed points, the spatial correlation is almost zero. The hyper-parameters for the prior of β were chosen such that its expected value was 3, representing the cubic root transformation recommended in the hydrological literature (Sansó and Guenni, 2000).

Following Bayes' Theorem, the posterior distribution is proportional to the likelihood times the prior distribution. For the spatio-temporal model in (9g)–(9k), the posterior distribution is given by

$$\begin{aligned} p(\sigma^2,\varsigma^2,\lambda,\beta,\boldsymbol{z},\boldsymbol{\theta}|\boldsymbol{X}) \propto{}& \left(\frac{1}{\sigma^2}\right)^{ST}\left(\frac{1}{\varsigma^2}\right)^{ST/2}|\boldsymbol{V}(\lambda)|^{-T/2} \\ &\times \exp\left(-\frac{1}{2\sigma^2}\sum_{t=1}^{T}\frac{1}{\varsigma^2}\|\boldsymbol{w}_t-\boldsymbol{z}_t\|^2\right. \\ &+(\boldsymbol{z}_t-\boldsymbol{F}'\boldsymbol{\theta}_t)'\boldsymbol{V}(\lambda)^{-1}(\boldsymbol{z}_t-\boldsymbol{F}'\boldsymbol{\theta}_t) \\ &\left.-\frac{1}{2}\sum_{t=1}^{T}(\boldsymbol{\theta}_t-\boldsymbol{G}\boldsymbol{\theta}_{t-1})'\boldsymbol{W}_t^{-1}(\boldsymbol{\theta}_t-\boldsymbol{G}\boldsymbol{\theta}_{t-1})\right) \\ &\times\left(\prod_{x_{it}>0}\frac{x_{it}^{1/\beta-1}}{\beta}\right)p(\boldsymbol{\theta}_0,\sigma^2,\varsigma^2,\lambda,\beta). \end{aligned} \tag{10}$$

From (10), we have the following full conditional distributions (f.c.d.): σ^2 and ς^2 are inverse gamma, $\boldsymbol{z}$ is multivariate normal, and $w_{ij}<0$ is a univariate truncated normal. The f.c.d. of λ and β do not have a known closed form. Since $\boldsymbol{\theta}_t$ are the state parameters of a normal dynamic model, their f.c.d. are multivariate normals.

For the dynamic models in (9a)–(9c) we also set independent priors to all the parameters. In particular, we considered normal prior distributions with zero mean and variance 10^3 for E_0, α and γ and a uniform distribution over [0,1] for ρ. For all the variance terms, $(\sigma_Y^2,\sigma_E^2,\sigma_W^2)$, we assigned inverse gamma distributions with both hyper-parameters equal to 0.01. When the gamma distribution is used to model the runoff, a gamma distribution with both parameters equal to 0.01 was used as a prior for ϕ, the shape parameter in (9a). In this case, the f.c.d. of the unknowns in (9a)–(9c) depend on the distribution assumed for Y_t and the hypothesis for $\sigma_E^2,\sigma_\alpha^2$ and σ_γ^2. In particular, if $p(\mu_t,\phi)$ is a gamma distribution and $\sigma_\alpha^2=\sigma_\gamma^2=0$, the f.c.d. of γ and σ_E^2 are normal and inverse gamma, respectively,

and the f.c.d. of α, ρ and ϕ do not have a known closed form.

Some computational details

In order to sample from the posterior distribution, we used a hybrid Gibbs sampling algorithm (Gelfand and Smith, 1990). Samples from the f.c.d. of λ, β, α and ρ were obtained through the slice sampling algorithm (Neal, 2003). We made use of a Metropolis–Hastings step to sample ϕ. Samples from $\boldsymbol{\theta}_t$ were obtained with the forward filtering backward sampling (FFBS) procedure (Frühwirth-Schnater, 1994). Following Sansó and Guenni (2000), we used discount factors for $\boldsymbol{W}_t$: $\delta_T = 0.90$ for the spatial trend and $\delta_S = 0.95$ for the seasonal effects. Finally for σ^2_α and σ^2_γ we used a discount factor of 0.95, whenever these parameters were considered in the model.

The MCMC algorithm for the spatio-temporal model was iterated 70000 times after a burn-in of 10000 steps, for two parallel chains. We stored every 10th iteration. For the runoff models we ran two chains for 60000 iterations, after a burn-in period of size 10000. The samples were taken at every 5th step. All the algorithms were written in `Ox` version 3.20 (see Doornik (2002)). The convergence of our chains was checked with the tests available in the `CODA` package, developed by Plummer et al. (2005), for the software `R` version 2.40.

Results

Taking advantage of the factorization of the likelihood in $p(Y_t|X_t)p(X_t)$, we used the computational routines for fitting the model in (3) with some different cases of polynomial trend, and then fitting several particular cases of the model in (1).

Our final model for rainfall has an intercept and a linear effect of longitude. Alternative models had shown that latitude has no significant effect in this region. The seasonal pattern was represented via two Fourier harmonics, which were chosen through an exploratory analysis of the periodogram of the series. Therefore matrix $\boldsymbol{F}_t$ in (9i) has row components: $(1, \text{longitude}(s_i), 1, 0, 1, 0)'$ and $\boldsymbol{G} = \text{diag}(\boldsymbol{G}_1, \boldsymbol{G}_2)$, where $\boldsymbol{G}_1$ is an identity matrix of order 2, and $\boldsymbol{G}_2$ has diagonal blocks

$$\boldsymbol{G}_{2r} = \begin{pmatrix} \cos(2\pi r/12) & \sin(2\pi r/12) \\ -\sin(2\pi r/12) & \cos(2\pi r/12) \end{pmatrix}, \quad r = 1, 2.$$

Fig. 3 shows the estimated paths of $\boldsymbol{\theta}_t$. We observe that the intercept clearly varies over time and seems to have an inter-annual cycle. The effect of longitude is negative

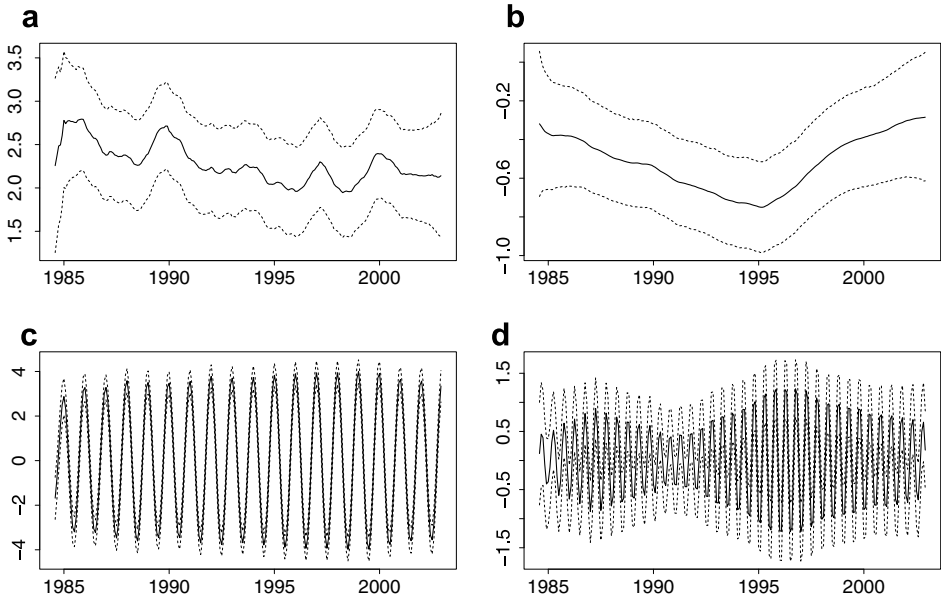

Figure 3 Estimated path of the state parameters for the rainfall model in (9k). Solid lines correspond to the posterior mean and dashed lines to the 95% posterior credible intervals.

Table 1 Posterior summaries associated with the parameters in equations (9g)–(9k)

Parameter	Mean	sd	2.5%	25%	50%	75%	97.5%	$\widehat{R}$
β	1.732	0.016	1.701	1.722	1.732	1.743	1.764	1.001
λ	0.045	0.007	0.033	0.040	0.044	0.050	0.061	1.001
ς^2	0.719	0.040	0.644	0.691	0.718	0.746	0.798	1.001
σ^2	1.100	0.044	1.015	1.070	1.098	1.128	1.191	1.003

and varies smoothly over time. The first harmonic has a very regular pattern, however the effect of the second harmonic exhibits two periods of different behaviors: before and after 1992. Table 1 presents the main summaries of the posterior samples obtained for the static parameters in equations (9g)–(9k). Note that we made inference about $\varsigma^2 = \tau^2/\sigma^2$. The posterior mean of β is 1.73, suggesting that the data is smoothly skewed, probably because we are working with monthly data. In Table 1 we also observe that the $\widehat{R}$ statistics (Gelman and Rubin, 1992) take values close to 1, suggesting that the convergence of our chains was reached.

In order to illustrate the fitted values produced by our spatio-temporal model, Fig. 4 displays the mean of the predictive posterior distribution of rainfall for two selected months. Note that different patterns are obtained for a rainy month (like December) and a dry month (like June).

The basin's rainfall was obtained by means of the spatial interpolations of rainfall over a grid of 63 points selected from a regular grid constructed over the whole basin under study. This grid is exhibited in Fig. 1a. Different grid's sizes were used and the results were not sensitive to this choice.The integral in (9f) was approximated by summing the 63 predicted values at each iteration of our MCMC algorithm. The resulting areal rainfall series, posterior mean and 95% credible intervals are displayed in Fig. 5. This figure also shows the mean areal precipitation estimated by the Thiessen method, a widely used deterministic method. It consists of assigning an area, or weight, called a Thiessen polygon, to each site. Then the individual weights are multiplied by the observed station and the values are summed up to obtain the areal average precipitation. Fig. 5 warrants attention because under the Bayesian framework we take into account the uncertainty involved and have a credible interval for each time. Therefore, this uncertainty will naturally be taken into account during the fitting of the runoff part of the model. Notice also that the estimated rainfall under the Thiessen method seems to be close to the upper limit of the posterior predictive interval. This suggests an overestimation of rainfall for some instants in time. This is also clear from the Q–Q plot presented on panel (b) of Fig. 5.

We used our posterior sample of the basin's rainfall to fit several particular cases of equations (9a)–(9c). Specifically, for $p(Y_t|X_t)$, we considered the two distribution mentioned above: log-normal and gamma. We also considered the following five specifications:

(a) The basic level, the transfer function and the instant rainfall effect are static; that is: $\sigma^2_\alpha = \sigma^2_\gamma = \sigma^2_E = 0, \forall t$.
(b) The basic level and the instant rainfall effect are static. The transfer function is stochastic: $\sigma^2_\alpha = \sigma^2_\gamma = 0$ and $\sigma^2_E > 0, \forall t$.
(c) The basic level follows a random walk. The transfer function and the instantaneous rainfall effect are static: $\alpha_t = \alpha_{t-1} + w_{\alpha,t}$, $\sigma^2_\alpha > 0$ and $\sigma^2_\gamma = \sigma^2_E = 0, \forall t$.
(d) The basic level is static, the transfer function is stochastic and the instantaneous rainfall effect follows

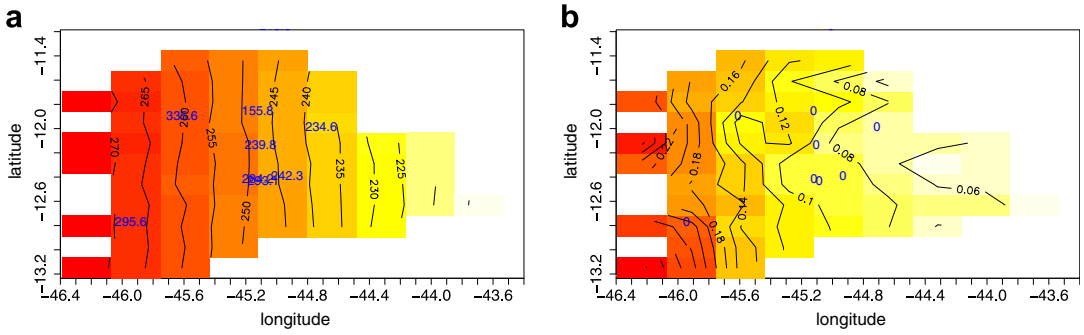

Figure 4 Posterior mean for rainfall for two different months. Dots mark the location of the rainfall monitoring stations. Darker values indicate higher rainfall values.

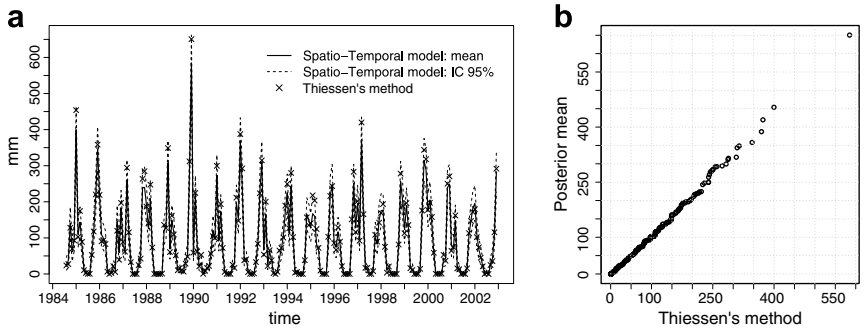

Figure 5 Panel (a): Areal rainfall (solid line corresponds to the posterior mean and dashed lines to the 95% credible interval. × corresponds to the Thiessen method estimation). Panel (b): Q–Q plot between the estimated rainfall over the basin obtained via the Thiessen's method and the posterior mean of the predictive distribution, as in Eq. (7).

a random walk: $\gamma_t = \gamma_{t-1} + w_{\gamma,t}$, $\sigma^2_\gamma > 0$, $\sigma^2_\alpha = 0$ and $\sigma^2_E > 0, \forall t$.

(e) The basic level is static, the transfer function is stochastic and the instantaneous rainfall effect varies over time following a constant trend and a seasonal pattern: $\gamma_t = \boldsymbol{G}_\gamma \gamma_{t-1} + w_{\gamma,t}$, $\sigma^2_\gamma > 0$, $\sigma^2_\alpha = 0$ and $\sigma^2_E > 0, \forall t$. $\boldsymbol{G}_\gamma = diag(1, \boldsymbol{G}_{2,\gamma})$, where

$$\boldsymbol{G}_{2,\gamma} = \begin{pmatrix} \cos(2\pi r/12) & \sin(2\pi r/12) \\ -\sin(2\pi r/12) & \cos(2\pi r/12) \end{pmatrix}, \quad r = 1, 2.$$

It is worth pointing out that we also fitted the function in (2b), however the results were less satisfactory than those under (2a) in terms of goodness of fit (to this particular dataset). Model comparison was performed using the following criteria: (i) Deviance Information Criterion (DIC), proposed by Spiegelhalter et al. (2001); (ii) Expected Predictive Deviation (EPD), proposed by Gelfand and Ghosh (1998); (iii) Mean Square Errors (MSE); and (iv) Mean Absolute Errors (MAE). In all cases, smaller values indicate the best model among those under study.

Table 2 (columns 4, 7, 8 and 9) shows the values of DIC, EPD (both considering a quadratic loss), MSE and MAE, computed for each of the five specifications described above. Two conclusions can be drawn from this table: first, all the criteria suggest that the gamma distribution should be chosen (this is no longer valid for columns 10 and 11); and second, in this case, specification (e) provides better results in terms of goodness of fit. It is worth mentioning that when using the rainfall time series obtained through the Thiessen's method as input (X_t) in the selected model, the values of DIC and EPD are 1817.6 and 90343, respectively. More specifically, as expected, the penalty term of both criteria is smaller, however the goodness of fit term is poorer. In other words, our joint model produces better results (fitted values) than the individual model that assumes rainfall as known. A similar conclusion is obtained when using just the posterior mean of the areal rainfall obtained from the spatio-temporal model.

Our final runoff model, therefore, assumes a gamma distribution with a static basic level, a stochastic transfer function and an instant rainfall effect varying across time following a constant trend and a seasonal pattern. In Figs. 6a and b we show the histograms of the samples from the posterior distributions of α and ρ, respectively. Fig. 6a shows the posterior mean of α is 4.84, indicating that the mean basic level in that region, during the observed time period, was 126.46 m^3/s. Fig. 6b shows that the mean of the regional recharge is 0.64 and varies between 0.57 and 0.71, which corresponds to the 95% posterior credible interval. Fig. 6c shows the evolution of the rainfall's instant effect, $\gamma_t X_t$. Remember that in the selected model, γ_t is a vector with five components where the first one corresponds to the constant trend and the last four correspond to the two harmonics used. Panel 6c shows the trajectory of the first component of γ_t. In this panel we observe that the rainfall's instant effect (without the seasonal effects) is always greater than zero and its value varies between 0.03 and 0.05. We also observe a decreasing trend for the last months.

One of the advantages of the Bayesian approach is that at the end of the inference procedure we have a sample from the posterior distributions of all the unknowns in the models. Therefore, it is straightforward to make inferences about functions of these quantities. The impulse-response function is probably one of the most important results of the class of models we proposed for runoff. This function indicates the intensity of the runoff response and how many periods the effect of a impulse of rainfall persists. For illustration purposes, and using the posterior sample of γ and ρ let us assume a window of 20 periods of time for which rainfall is zero for all times except when $t = 5$, i.e. $X_5 = 1$. Panel (a) of Fig. 7 shows the persistence of rainfall over runoff for this setting. The estimated decay rate is clearly shown, the effect of rainfall dies off after $t = 10$. Also, the advantage of using the Bayesian paradigm is clear, the dotted lines describe the 95% posterior credible intervals of the impulse-response function for each time t, and the grey vertical lines represent the posterior sample of the function for

Table 2 Model comparison criteria for three alternative specifications of (9a)–(9c): deviance information criteria (DIC), expected predictive deviance (EPD), mean square error (MSE) and mean absolute error (MAE)

Model	DIC	EPD	MSE[a]	MAE[a]	MSE[b]	MAE[b]
Log-normal distribution for runoff (Y_t)						
(a)	1 945.3	198 423	429.1	14.9	1 366.9	27.5
(b)	1 833.0	91 674	149.9	7.4	1 359.3	26.8
(c)	1 849.9	130 231	292.1	10.3	2 058.4	27.5
(d)	1 843.9	102 939	186.5	8.4	1 588.6	25.7
(e)	2 007.3	186 433	274.2	9.7	1 596.4	26.2
Gamma distribution for runoff (Y_t)						
(a)	1 934.6	197 570	427.5	14.8	1 398.6	26.5
(b)	1 829.1	84 514	134.3	7.0	1 119.6	26.0
(c)	1 838.1	135 407	280.2	10.0	2 078.2	28.0
(d)	1 831.6	86 602	139.0	7.2	1 434.8	26.8
(e)	1 817.9	70 457	88.8	5.6	1 583.0	26.5

[a] With fitted values: in the sample, (221 months).
[b] With predicted values: out-of-sample. (21 months).

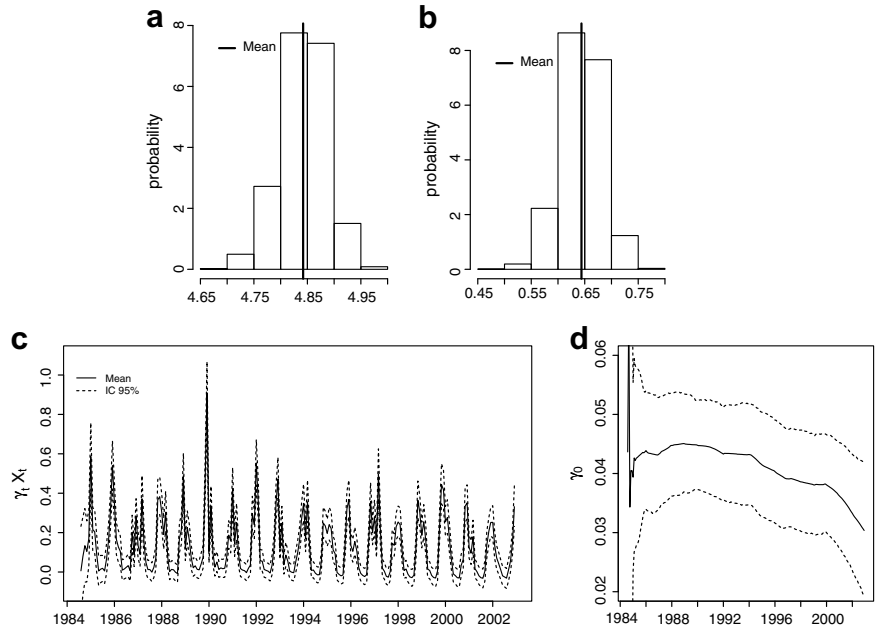

Figure 6 Parameters in (9a)–(9c), with specification (e) and gamma response.

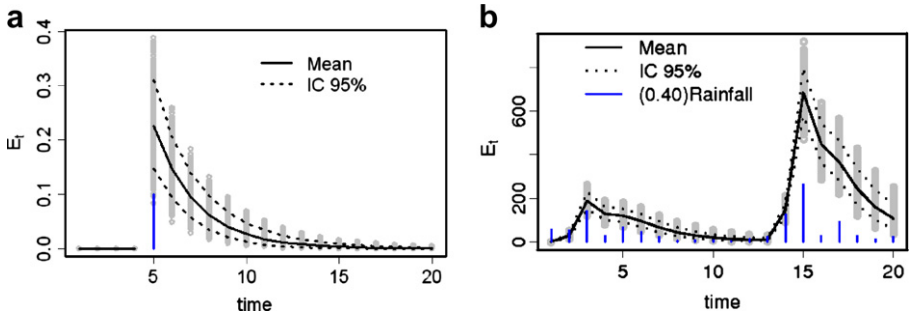

Figure 7 Runoff impulse–response functions. For both panels, solid lines represents the mean and dotted lines represent the 95% posterior credible interval of the response function for each time t. Panel (a) corresponds to a hypothetical situation with 20 periods of time, where rainfall equals zero for all times, except for $t = 5$, that is $X_5 = 1$. Panel (b) shows the summary of the impulse-response function for the initial 20 periods of time for our dataset. Vertical lines represent the values of rainfall multiplied by 0.40.

each time t. Similarly, Panel (b) shows the summary of the impulse-response function for the 20 initial periods of time for our rainfall–runoff dataset. In this figure, vertical lines represent the amount of rainfall for each period of time. For visualization (scale) reasons we multiplied the value of rainfall by 0.40.

Fig. 8a shows the fitted values obtained for the 221 months in the runoff series. Note that the observed runoff

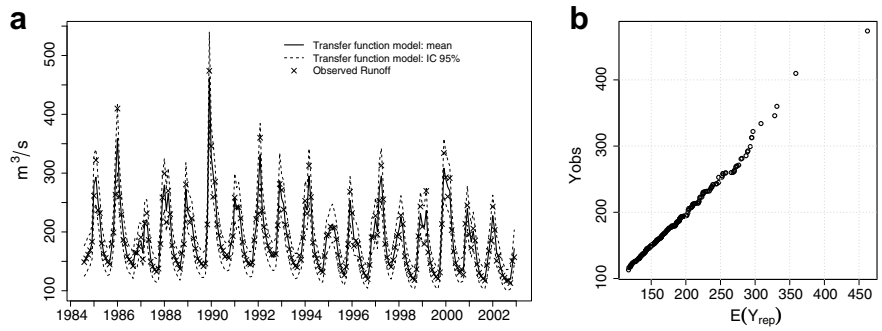

Figure 8 Runoff fitted values, under Model (9a)–(9c). The solid line corresponds to the posterior mean and dashed lines to the limits of the 95% credible interval. × corresponds to observed data.

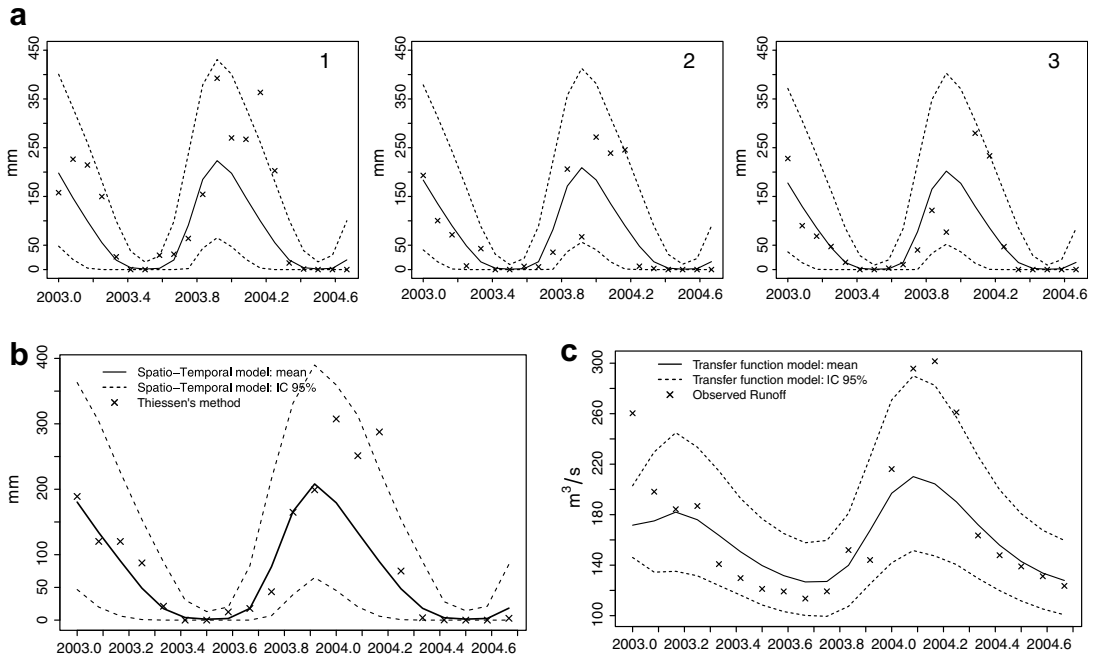

Figure 9 Rainfall—Runoff forecast values. Mean (solid lines) and 95% credible interval (dashed lines) of predictive distributions. *x*: in (a) and (c) correspond to the observed data, in (b) corresponds to the values obtained with the Thiessen method.

values are within the limits of the 95% interval of the posterior predictive distribution, indicating an acceptable overall fit. However, it can be observed that the higher observed values (over 300 m^3/s) are near the upper limit, suggesting the use of an extreme value distribution to model them. This lack of fit at the upper tail is also revealed by the Q—Q plot among observed values and posterior predictive means displayed in Fig. 8a.

Temporal predictions and spatial interpolations

An important issue to be considered here is that fitted and forecast values obtained from Bayesian rainfall—runoff models can be used in synthetic hydrology. As pointed out by Rios-Insua et al. (2002), the sample of the predictive distributions can be used to simulate sequences of observations that mimic some behavior phenomenon for engineering design or analysis. Therefore, good interpolated and forecast values are important to support other areas of hydrological research.

In order to evaluate the interpolations and predictions obtained with our models, we left the last 21 observations out of the sample. The predictive distribution of rainfall was used to forecast the precipitation at each monitoring station. Also, as we stated in Section ''A simultaneous model for rainfall—runoff'', at each iteration of the MCMC algorithm, we used the predictive distribution of rainfall to compute the areal one and then we forecast the runoff.

From columns 10 and 11 of Table 2, we conclude that the selected model (gamma distribution and specification (e)) does not exhibit the smallest out-of-sample MSE and MAE. However, we used that model to make our temporal predictions because the MAE values are very similar among the considered models. Fig. 9a shows the temporal predictions obtained for three of the nine rainfall stations, the temporal areal prediction for the areal rainfall is presented in Fig. 9b, and the predicted series for runoff is displayed in Fig. 9c. Note that almost all of the true values are within the limits of the 95% posterior credible interval provided by our approach.

Concluding remarks

In this paper we proposed a joint model for rainfall and runoff, by taking into account all the uncertainty associated with both stochastic processes and considering their different spatial units. We used some previously established individual models whose parameters have natural physical interpretations. We also fitted the data in their original scale. Under a Bayesian framework we proposed to fit non-normal (gamma) transfer function models using the CUBS sampling scheme that significatively reduces the computational time and is easy to implement. We were also careful with the implementation of the MCMC algorithm. Although it is not shown here, missing data are naturally handled as parameters of the models. We believe our approach is a promising tool for runoff—rainfall analysis.

As pointed out by the referees, we need alternative approaches to tackle the problem of poor fitting at the runoff peaks. One way to do this is to consider extreme values distributions which will be able to capture extreme events. Or even consider mixture of distributions as suggested by Behrens et al. (2004). Or as suggested by one of the referees, one might consider a more adequate transfer function, one for the rainy season and another one for the dry season. This is part of our current investigation.

A natural extension of the model proposed here is the inclusion of a variable that represents the region's vegeta-

tion. Vegetation controls the evapotranspiration and interceptation processes, two components of the water balance.

Natural alternatives to the models used here are to consider other transfer functions for the runoff and to consider other spatial correlation functions in the spatio-temporal model for rainfall. An interesting extension is the use of hierarchical dynamic models (like Gamerman and Migon (1993)), to model a set of runoff series from different basins but with similar geological and climate characteristics. Also, linear models can be considered for both parameters of the biparametric gamma distribution used for runoff, as in Capkun et al. (2001).

Finally, the results obtained with our approach provide an important input to the decision problem of reservoir operations (see Rios-Insua et al. (1997)), which is just one of the topics of our current research.

Acknowledgements

The work of Romy R. Ravines was supported by *Coordenação de Aperfeiçoamento de Pessoal de Ensino Superior* (CAPES-Brazil). Alexandra M. Schmidt and Helio S. Migon were supported by *Conselho Nacional de Desenvolvimento Científico e Tecnológico* (CNPq-Brazil). The authors thank the *Laboratório de Hidrologia* of the *Universidade Federal do Rio de Janeiro* (UFRJ), Brazil for providing the Rio Grande basin data. The authors thank the Associate Editor George Vachaud, and two anonymous referees whose comments improved the presentation of the paper.

Appendix A. Likelihood and Spatial Change of Support

Here we present in more detail the computations for the change of support problem. Let $\boldsymbol{Y} = (Y_1, \ldots, Y_T)'$, $\boldsymbol{X} = (X_1, \ldots, X_T)'$, and $\boldsymbol{X}(s_i) = (X_1(s_i), \ldots, X_T(s_i))'$. Also, consider $\boldsymbol{X}_t(\boldsymbol{s}) = (X_t(s_1), \ldots, X_t(s_S))'$ and $\boldsymbol{X}(\boldsymbol{s}) = (\boldsymbol{X}_1(\boldsymbol{s}), \ldots, \boldsymbol{X}_T(\boldsymbol{s}))$ an $S \times T$ matrix, where $\boldsymbol{s} = (s_1, \ldots, s_S)$. The joint distribution of $\boldsymbol{Y}$ and $\boldsymbol{X}(s)$ is given by

$$\underbrace{p(\boldsymbol{Y}, \boldsymbol{X}(\boldsymbol{s})|\boldsymbol{\Theta})}_{\text{observed data}} = \int p(\boldsymbol{Y}, \boldsymbol{X}|\boldsymbol{X}(s), \boldsymbol{\Theta}) p(\boldsymbol{X}(\boldsymbol{s})|\boldsymbol{\Theta}) \underbrace{\mathrm{d}\boldsymbol{X}}_{\text{latent process}}$$
$$= \int p(\boldsymbol{Y}|\boldsymbol{X}, \boldsymbol{X}(\boldsymbol{s}), \boldsymbol{\Theta}_Y) \times \underbrace{p(\boldsymbol{X}, \boldsymbol{X}(\boldsymbol{s})|\boldsymbol{\Theta}_X)}_{\text{Monte Carlo approximation}} \mathrm{d}\boldsymbol{X}, \quad \text{(A1)}$$

where $\boldsymbol{\Theta} = (\boldsymbol{\Theta}_Y, \boldsymbol{\Theta}_X)$. Actually, the joint distribution of the observed data is given by $p(\boldsymbol{Y}, \boldsymbol{X}(\boldsymbol{s})|\boldsymbol{\Theta})$, then $\boldsymbol{X}$ plays the role of a latent variable. Since one of the advantages of the use of MCMC methods is that we can sample $p(\boldsymbol{Y}, \boldsymbol{X}, \boldsymbol{X}(\boldsymbol{s})|\boldsymbol{\Theta})$ and consider that samples from $p(\boldsymbol{Y}, \boldsymbol{X}(\boldsymbol{s}))$ belong to the marginal joint distribution of both variables, we are concerned with $p(\boldsymbol{Y}, \boldsymbol{X}, \boldsymbol{X}(\boldsymbol{s})|\boldsymbol{\Theta})$, which for a fixed t is given by

$$p(Y_t, X_t, \boldsymbol{X}_t(\boldsymbol{s})|\boldsymbol{\Theta}) = p(Y_t|X_t, \boldsymbol{X}_t(\boldsymbol{s}), \boldsymbol{\Theta}_Y) p(X_t, \boldsymbol{X}_t(\boldsymbol{s})|\boldsymbol{\Theta}_X). \quad \text{(A2)}$$

Now, we focus on $p(X_t, \boldsymbol{X}_t(\boldsymbol{s})|\boldsymbol{\Theta}_X)$. Recall that

$$X_t = \int_B \boldsymbol{X}_t(\boldsymbol{s}) \mathrm{d}\boldsymbol{s}, \quad \text{(A3)}$$

that is, X_t is a ''function'' of $\boldsymbol{X}_t(\boldsymbol{s})$ and the predictive distribution of X_t is

$$\underbrace{p(X_t|\boldsymbol{X}_t(\boldsymbol{s}))}_{\text{predictive}} = \int p(X_t|\boldsymbol{X}_t(\boldsymbol{s}), \boldsymbol{\Theta}_X) \underbrace{p(\boldsymbol{\Theta}_X|\boldsymbol{X}_t(\boldsymbol{s}))}_{\text{posterior}} \mathrm{d}\boldsymbol{\Theta}_X. \quad \text{(A4)}$$

The moments of $p(X_t|\boldsymbol{X}_t(\boldsymbol{s}))$ in (A4) involve integrals with respect to $\boldsymbol{s}$. For instance, assuming that the joint distribution of X_t and $\boldsymbol{X}_t(\boldsymbol{s})$ is normal, we have

$$E(X_t|\boldsymbol{\Theta}_X) = \int_B E(\boldsymbol{X}_t(\boldsymbol{s})|\boldsymbol{\Theta}_X) \mathrm{d}\boldsymbol{s}. \quad \text{(A5)}$$

Gelfand et al. (2001) proposed to approximate those moments by means of Monte Carlo integration. They showed that

$$\hat{p}((X_t, \boldsymbol{X}_t(\boldsymbol{s}))'|\boldsymbol{\Theta}_X) = p((\widehat{X}_t, \boldsymbol{X}_t(\boldsymbol{s}))'|\boldsymbol{\Theta}_X), \quad \text{(A6)}$$

where $\hat{}$ denotes a Monte Carlo integration and

$$\widehat{X}_t = \sum_{i=1}^{S_B} \widehat{X}_t(s_i) \quad i = 1, \ldots, S_B. \quad \text{(A7)}$$

According to Gelfand et al. (2001), (A6) implies that the approximated joint density of X_t and $\boldsymbol{X}_t(\boldsymbol{s})$ is equal to the joint density of $\widehat{X}_t$ and $\boldsymbol{X}_t(\boldsymbol{s})$, so, in practice, $\widehat{X}_t$ is the one to be sampled. The authors stated that $\widehat{X}_t \to^P X_t$ if $\boldsymbol{X}_t(\boldsymbol{s})$ is almost surely a continuous process.

References

Behrens, C., Lopes, H., Gamerman, D., 2004. Bayesian analysis of extreme events with threshold estimation. Statistical Modelling 4, 227–244.

Capkun, G., Davison, A.C., Musy, A., 2001. A robust rainfall–runoff transfer model. Water Resources Research 37, 3207–3216.

Cressie, N., 1993. Statistics for Spatial Data. Wiley & sons, NY.

Doornik, J., 2002. Object-Oriented Matrix Programming Using Ox, third ed. Timberlake Consultants Press and Oxford, London <http://www.nuff.ox.ac.uk/Users/Doornik>.

Fernandes, M.V., Schmidt, A.M., Migon, H.S., in press. Modelling zero-inflated spatio-temporal processes. Technical report. Statistical Modelling: an International Journal.

Frühwirth-Schnater, S., 1994. Data augmentation and dynamic linear models. Journal of Time Series Analysis 15, 183–202.

Gamerman, D., Lopes, H.F., 2006. Markov Chain Monte Carlo: Stochastic Simulation for Bayesian Inference. Chapman & Hall/CRC, NY.

Gamerman, D., Migon, H., 1993. Dynamic hierarquical models. Journal of the Royal Statistical Society, B 85, 629–642.

Gelfand, A.E., Ghosh, S., 1998. Model choice: a minimum posterior predictive loss approach. Biometrika 85, 1–11.

Gelfand, A.E., Smith, A., 1990. Sampling-based approaches to calculating marginal densities. Journal of the American Statistical Association 85, 398–409.

Gelfand, A.E., Zhu, L., Carlin, B., 2001. On the change of support problem for spatio-temporal data. Biostatistics 2, 31–45.

Gelman, A., Rubin, D., 1992. Inference from iterative simulation using multiple sequences. Statistical Science 7, 457–511.

Lu, Z.-Q., Berliner, L.M., 1999. Markov switching time series models with application to a daily runoff series. Water Resources Research 35, 523–534.

Migon, H., Harrison, J., 1985. An application of nonlinear Bayesian forecasting to television advertising. In: Bernardo, J., DeGroot, M., Lindley, D., Smith, A. (Eds.), Bayesian Statistics, vol. 2. Elsevier Science Publishers B.V., North-Holland, pp. 681–696.

Migon, H., Monteiro, A.B., 1997. Rain-fall modelling: an application of Bayesian forecasting. Stochastic Hydrology and Hydraulics 11, 115—127.

Neal, R., 2003. Slice sampling (with discussion). Annals of Statistics 31, 705—767.

Plummer, M., Best, N., Cowles, K., Vines, K., 2005. CODA: Output analysis and diagnostics for MCMC. R package version 0.9-5, <http://www-fis.iarc.fr/coda/>.

Ravines, R., Migon, H., Schmidt, A., 2007. An efficient sampling scheme for generalized dynamic models. Working paper, Departamento de Métodos Estatísticos, Universidade Federal do Rio de Janeiro.

Rios-Insua, D., Salewiz, K., Müller, P., Bielza, C., 1997. Bayesian methods in reservoir opeations: the Zambezi river case. In: French, S., Smith, J. (Eds.), The practice of Bayesian Analysis. Arnold, pp. 107—130.

Rios-Insua, D., Montes, R., Palomo, J., 2002. Bayesian methods in hydrology: a review. Revista de la Real Academia de Ciencias. Serie A. Matemática 96, 461—479.

Sales, P., 1989. Procedimentos lineares para identificação e estimação de parâmetros de modelos para séries temporais uni e multivariadas. Ph.D. thesis, Engenharia de Produção, COPPE - UFRJ, Rio de Janeiro, Brazil. (in Portuguese).

Sansó, B., Guenni, L., 2000. A non-stationary multi-site model for rainfall. Journal of the American Statistical Association 95, 1089—1100.

Schmidt, A.M., Gelfand, A.E., 2003. A Bayesian coregionalization approach for multivariate pollutant data. Journal of Geophysical Research-Atmospheres, 108.

Spiegelhalter, D., Best, N., Carlin, B., der Linde, A.V., 2001. Bayesian measures of model complexity and fit. Journal of the Royal Statistical Society, B 64, 583—639.

Velarde, L., Migon, H., Pereira, B., 2004. Space time modeling of non-negative variables with point of mass at zero. Environmetrics 15, 561—576.

West, M., Harrison, J., 1997. Bayesian Forecasting and Dynamic Models, second ed. Springer-Verlag, NY.

West, M., Harrison, J., Migon, H., 1985. Dynamic generalized linear models and Bayesian forecasting. Journal of the American Statistical Association 80, 73—83.